PAPER Special Section on Machine Vision and its Applications

Multiple Human Tracking Using an Omnidirectional Camera with Local Rectification and World Coordinates Representation

Hitoshi NISHIMURA[†,††a)], Naoya MAKIBUCHI[†b)], Kazuyuki TASAKA[†c)],
Yasutomo KAWANISHI[†,††d)], *Members*, *and* Hiroshi MURASE[†,††e)], *Fellow*

SUMMARY Multiple human tracking is widely used in various fields such as marketing and surveillance. The typical approach associates human detection results between consecutive frames using the features and bounding boxes (position+size) of detected humans. Some methods use an omnidirectional camera to cover a wider area, but ID switch often occurs in association with detections due to following two factors: i) The feature is adversely affected because the bounding box includes many background regions when a human is captured from an oblique angle. ii) The position and size change dramatically between consecutive frames because the distance metric is non-uniform in an omnidirectional image. In this paper, we propose a novel method that accurately tracks humans with an association metric for omnidirectional images. The proposed method has two key points: i) For feature extraction, we introduce local rectification, which reduces the effect of background regions in the bounding box. ii) For distance calculation, we describe the positions in a world coordinate system where the distance metric is uniform. In the experiments, we confirmed that the Multiple Object Tracking Accuracy (MOTA) improved 3.3 in the LargeRoom dataset and improved 2.3 in the SmallRoom dataset.

key words: *multiple human tracking, data association, omnidirectional camera*

1. Introduction

Multiple human tracking is a fundamental technique and widely used in various fields such as marketing, surveillance, and virtual reality. The task of multiple human tracking is to achieve continuous detection of multiple humans while maintaining their identities (ID) given time-series images [1]. In a large-scale practical system, one approach that is efficient is to transmit captured images to a server and process them collectively. In such a system, it is expected that the frame rate is low in terms of keeping bandwidth or data storage.

Most state-of-the-art tracking methods [2]–[7] are based on a tracking-by-detection approach owing to detection accuracy improvement. The tracking-by-detection approach achieves multiple human tracking by iterative data association [8]. The data association matches detection results between consecutive frames with an association metric.

Human detection is making remarkable advances based on deep learning (e.g. Faster R-CNN [9], YOLO [10], and SSD [11]), and the detection accuracy has significantly improved. The use of Convolutional Neural Networks (CNNs) is one of the most important deep learning methods, and can extract powerful discriminative feature representations. Most tracking-by-detection approaches use both features and bounding boxes (position+size) for the association metric, and utilize CNNs for feature extraction and bounding box estimation. In this work, we employ powerful deep learning methods.

Conventional deep-learning-based tracking methods [2]–[7] have commonly used a normal camera. In addition to a normal camera, in recent years, an *omnidirectional* camera has been used for tracking. The omnidirectional camera has a 360-degree view, and can cover a wide area using a single camera. Therefore, the omnidirectional camera reduces initial costs and subsequent maintenance costs (e.g. costs associated with setup, labor, repairs, and software licensing) compared to those of a normal camera. In this study, we utilize only one omnidirectional camera.

However, it is difficult to simply apply the deep-learning-based tracking method [2]–[7] to an omnidirectional image. While omnidirectional images have serious *distortions*, most deep-learning-based detection methods [9]–[11] estimate the human region as a simple axis-aligned bounding box. When applying these methods to omnidirectional images, ID switch, which means the target human ID changes to another ID, often occurs. ID switch occurs due to following two factors. i) The feature is adversely affected because the bounding box includes many background regions when a human is captured from an oblique angle (Fig. 1 (a)). ii) The position and size change dramatically between consecutive frames because the distance metric is non-uniform (Fig. 1 (b)).

Some tracking methods use omnidirectional cameras exclusively. Most of them rectify the entire omnidirectional image (expand to a panoramic image, hereinafter, *global rectification*) before initiating tracking [12]–[18]. In the rectified image, the angle of the human can be normalized. However, the bounding box includes many background regions because there is serious distortion when the human's position is around the center in the original image.

Manuscript received August 30, 2019.
Manuscript revised February 14, 2020.
Manuscript publicized April 10, 2020.

[†]The authors are with KDDI Research, Inc., Fujimino-shi, 356–8502 Japan.

[††]The authors are with Graduate School of Informatics, Nagoya University, Nagoya-shi, 464–8601 Japan.

a) E-mail: ht-nishimura@kddi-research.jp
b) E-mail: na-makibuchi@kddi-research.jp
c) E-mail: ka-tasaka@kddi-research.jp
d) E-mail: kawanishi@is.nagoya-u.ac.jp
e) E-mail: murase@nagoya-u.jp

DOI: 10.1587/transinf.2019MVP0009

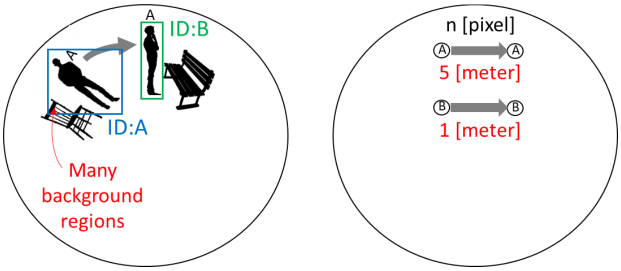

(a) Background region ratio in a bounding box varies depending on the position in the image.

(b) Distance in the real-world corresponding to *n* pixels varies depending on the position in the image.

Fig. 1 ID switch is caused by two factors because an omnidirectional image has serious distortions.

Table 1 Related work in terms of camera, rectification, and tracking-by-detection. Details of A), B), and C) are described in Sect. 2.

	Camera	Rectification	Tracking-by-detection
A) [2]–[7]	Normal	-	Yes
B) [12]–[18]	Omni	Global rectification	No
C) [19]–[22]	Omni	-	No
Ours	Omni	Local rectification	Yes

Therefore, the above two factors illustrated in Fig. 1 are not solved.

In this paper, we propose a novel method that accurately tracks humans with an association metric for omnidirectional images. Note that the proposed method works for omnidirectional images captured by a camera fixed on the ceiling. The proposed method has two key points: i) For feature extraction, we introduce *local rectification*, which rectifies the human regions locally (not the overall image). It reduces the effect of background regions in the bounding box. ii) For distance calculation, we describe the positions in a *world coordinate* system where the distance metric is uniform. The proposed method (above two points) can be added to other arbitrary state-of-the-art trackers and improve the tracking accuracy of those trackers.

Our main contributions are as follows:

- We propose local rectification for reducing the effect of background regions when extracting features.
- We describe the human position in a world coordinate system where the distance metric is uniform.
- For above two contributions, we utilized a 3D-human model which is robust against unstable human detection.

The rest of the paper is organized as follows. First, we review related work in Sect. 2. Then, we describe the proposed method in Sect. 3, and conduct the experiments in Sect. 4. Finally, we conclude our work in Sect. 5.

2. Related Work

In this section, we review multiple human tracking methods in relation to the type of camera, rectification, and use of deep learning. Table 1 shows related work compared to ours.

A) Many state-of-the-art tracking methods use normal cameras [2]–[7] and are based on a tracking-by-detection framework. Bewley *et al.* proposed SORT, which utilizes only bounding boxes for data association [2]. Wojke *et al.* extended SORT [2], and data association is performed using not only the bounding boxes but also features [3]. Both features and bounding boxes are estimated by deep learning.

B) Many methods that globally rectify omnidirectional images before the tracking have been proposed [12]–[18]. In a globally rectified image, the angle of the human can be normalized. Gächter utilized the temporal and background change detection [12]. Cielniak *et al.* proposed a method that performs human extraction and applies a Kalman filter [14]. Liu *et al.* proposed a method that detects a human based on a background model, and a greedy data association is performed [13]. Kobilarov *et al.* introduced a method that utilizes a Kanade Lucas Tomasi (KLT) tracker and performs data association with a Probabilistic Data Association Filter (PDAF) [15]. Song *et al.* proposed a method that rectifies only part of the outside image, and a human is tracked using a particle filter [16]. Kawasaki *et al.* combined static and dynamic background subtraction [17] for the human tracking. Delforouzi *et al.* introduced a method that can detect unknown objects based on a Training-Learning-Detection (TLD) scheme [18]. Yao *et al.* proposed a method that applies vertical vanishing point mapping to a normal image [23]. These methods reduce the dramatic changes in the bounding box position between consecutive frames if a human moves in the horizontal axis direction in the rectified image.

C) Several methods track humans in omnidirectional images without rectification [19]–[22]. Chen *et al.* proposed a method that tracks a human by Markov Random Fields (MRF) [19]. Zhang *et al.* proposed a method that extracts a human region by matching the foreground region and 3D-human model [22]. The foreground region is estimated by background subtraction. Rameau *et al.* introduced a method that tracks humans using a particle filter, the state vector of which is based on a sphere [20]. Cinaroglu *et al.* proposed a method that detects humans using a sliding window based on a Riemannian metric [21].

In A), ID switch often occurs due to following two factors. i) While images captured by the omnidirectional camera have serious distortions, most deep-learning-based detection methods estimate only a simple axis-aligned bounding box. The feature is adversely affected because the bounding box includes many background regions and the human's angles vary when a human is captured from an oblique angle. Although semantic segmentation methods [24], [25] can be used for background reduction, they incur a heavy computational cost. ii) The position and size change dramatically because the distance metric is non-uniform. In B), the bounding box includes many background regions because the area around the center of the image is excessively expanded. In C), since most methods are not based on the tracking-by-detection approach, it is difficult to incorporate existing deep-learning-based detectors that rely on normal images.

3. Proposed Method

The proposed method has two keypoints. i) We introduce local rectification, which rectifies only the human region in order to reduce the effect of background regions. ii) We describe the positions in the world coordinates where the distance metric is uniform in order to avoid dramatical changes in the position and shape.

The proposed method is based on the tracking-by-detection approach. The overall process of the proposed method is shown in Fig. 2. After the targeted humans are detected in the image coordinates (Sect. 3.1), the association metric is calculated (Sect. 3.2). Using the metric, these humans are tracked by data association (Section 3.3). The original feature of the proposed method is the association metric explained in Sect. 3.2. The regions are locally rectified and the features are extracted from the regions (Sect. 3.2.2). Also, the positions of the targeted humans are estimated in the world coordinates (Sect. 3.2.3).

Before describing the proposed method in detail, allow me to formalize the multiple human tracking. Let $\mathbf{o}^f$ be an omnidirectional image at frame f. Let $T^f = (\mathbf{t}_1^f, \mathbf{t}_2^f, \cdots, \mathbf{t}_{N_t}^f)$ be tracklets at frame f, where $\mathbf{t}_i^f$ is the i-th tracklet. Let $B^f = (\mathbf{b}_1^f, \mathbf{b}_2^f, \cdots, \mathbf{b}_{N_b}^f)$ be bounding boxes at frame f, where $\mathbf{b}_j^f$ is the j-th bounding box. The multiple human tracking is formalized as the problem of sequentially estimating T^f where T^{f-1} and $\mathbf{o}^f$ are given.

3.1 Human Detection in Image Coordinates

For each frame f, humans are detected by the deep-learning-based detection method. Each bounding box $\mathbf{b}_j^f$ is defined as a *normal* rectangle, and is represented by $\mathbf{n} = (x, y, w, h)$. x and y are the x-axis and y-axis in the upper left of the rectangle in an omnidirectional image. w and h are the width and height of the rectangle in an omnidirectional image. $\mathbf{n}$ is calculated using a human detector. Although we chose SSD [11] for the detector in this work, any other detector can be used. The detector is trained using omnidirectional images in advance.

3.2 Proposed Association Metric

The local rectification (Sect. 3.2.2) and human position estimation in the world coordinates (Sect. 3.2.3) are performed using the bounding boxes obtained in Sect. 3.1. Before these estimations, the estimator is trained in advance (Sect. 3.2.1),

In the proposed method, the bounding box $\mathbf{b}_j^f$ is defined as a *rotated* rectangle, and is represented by $\mathbf{r} = (x_r, y_r, w_r, h_r, \phi)$. x_r and y_r are the x-axis and y-axis of the center position of the rectangle. w_r and h_r are the width and height of the rectangle. ϕ is an angle that is oriented clockwise. The positive direction of the horizontal axis is defined as $\phi = 0$. The domain of ϕ is $0 \leq \phi < 2\pi$. x_r and y_r are set as the center of rotation.

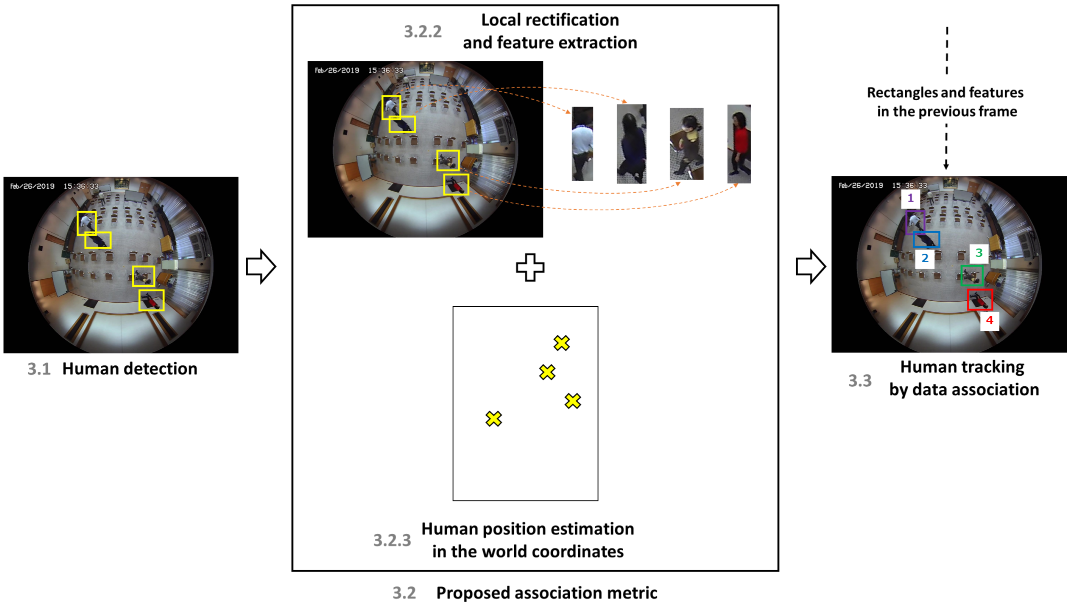
3.2.2 Local rectification and feature extraction
Rectangles and features in the previous frame
3.1 Human detection
1
2
3
4
3.3 Human tracking by data association
3.2.3 Human position estimation in the world coordinates
3.2 Proposed association metric

Fig. 2 Overall process of the proposed method. First, the targeted humans are detected in the image coordinates. Second, the regions are locally rectified, and the features are extracted from the regions. At the same time, the positions of the targets are estimated in the world coordinates. Finally, these humans are tracked by data association using the features and positions of the targeted humans.

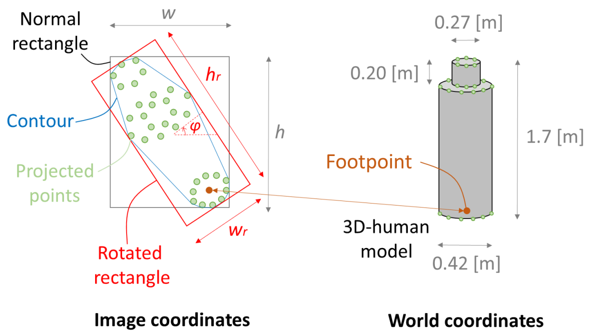

Fig. 3 A 3D-human model is virtually located in the world coordinates, and a human contour that consists of points is calculated in the image coordinates. Then a normal rectangle and a rotated rectangle are calculated in the image coordinates.

3.2.1 Training of Rotated Rectangle and Human Position Estimator

This section describes the method of training the rotated rectangle and human position estimator. The input of the estimator is a normal rectangle $\mathbf{n} = (x, y, w, h)$ obtained in Sect. 3.1. The output of the estimator is rotated rectangle $\mathbf{r} = (x_r, y_r, w_r, h_r, \phi)$ and a position in the world coordinates $\mathbf{q} = (q_1, q_2, 0)$.

The detection result, $\mathbf{n}$, estimated in Sect. 3.1 is unstable because an omnidirectional image has serious distortions. In order to refine the unstable detection result, we utilized a 3D-human model [22], [26], [27] for training the estimator. The human regions in various positions are calculated using the 3D-human model. Using these human regions, the rotated rectangles and the footpoint of the targeted human are registered. In this paper, we use a simple 3D-human model that consists of two cylinders (Fig. 3).

For utilizing the 3D-human model, the projection between the image coordinates and the world coordinates is important. $\mathbf{p} = (p_1, p_2)$ denotes a position in the image coordinates, and elements of $\mathbf{p}$ are values of the x-axis and y-axis. Also, we denote a position in the world coordinates as $\mathbf{q} = (q_1, q_2, q_3)$, and elements of $\mathbf{q}$ are values of the x-axis, y-axis, and z-axis. The projection from world to the image coordinates is performed using the camera projection matrix $M \in \mathbb{R}^{3\times4}$ [28].

$$\lambda \cdot \mathbf{p}^{\mathsf{T}} = M\mathbf{q}^{\mathsf{T}}. \tag{1}$$

A virtual 3D-human model in the world coordinates and a human contour in the image coordinates are shown in Fig. 3. Human regions are associated via a footpoint of the human between the image coordinates and the world coordinates. For each footpoint $\mathbf{p} = (p_1, p_2)$ in the image coordinates, the following set of procedures is repeated ($1 \leq p_1 \leq 1280, 1 \leq p_2 \leq 960$).

- $\mathbf{p}$ is projected to $\mathbf{q} = (q_1, q_2, q_3)$ in the world coordinates by Eq. (1), and a footpoint is determined as $\mathbf{q} = (q_1, q_2, 0)$.
- A 3D-human model is virtually located in the world coordinates according to $\mathbf{q}$.
- A human contour that consists of points is calculated in the image coordinates using the located 3D-human model. Each vertex in the world coordinates is projected into the image coordinates by Eq. (1).
- A normal rectangle $\mathbf{n} = (x, y, w, h)$ and a rotated rectangle $\mathbf{r} = (x_r, y_r, w_r, h_r, \phi)$ are calculated in the image coordinates using the human contour. Both rectangles are calculated as a circumscribed rectangle of the human contour in terms of rectangle area minimization.
- The correspondence between a query vector $\mathbf{n}$ and a rotated rectangle $\mathbf{r}$ is registered. Also, the correspondence between the query vector $\mathbf{n}$ and a footpoint $\mathbf{q}$ is registered.

Since the query vectors obtained in these procedures do not cover all possible $\mathbf{n}$, we employ a nearest neighbor search. Kd-tree [29] is utilized to accelerate the nearest neighbor search. Therefore, if a query vector is input, we can obtain the corresponding rotated rectangle and footpoint efficiently.

3.2.2 Local Rectification and Feature Extraction in Image Coordinates

Local rectification consists of estimating the rotated rectangle and rotating it. The rotated rectangle $\mathbf{r} = (x_r, y_r, w_r, h_r, \phi)$ is calculated by the estimator using a query vector $\mathbf{n}$. The rotated rectangle $\mathbf{r}$ is rotated to be $\phi = 0$ in order that the footpoint is always in the lower part. The rotation is performed by the following rotation matrix:

$$R = \begin{pmatrix} \alpha & -\beta & (1-\alpha)x_r - \beta y_r \\ \beta & \alpha & \beta x_r - (1-\alpha)y_r \end{pmatrix}, \tag{2}$$
$$\alpha = cos(-a),\ \beta = sin(-a),$$

where a is an angle of rotation described later. x_r and y_r are set as the center of rotation.

Then, the feature $\mathbf{a}$ corresponding to the rectangle $\mathbf{b}$ is calculated. Since the image is locally rectified (reduce background regions and normalize the human angle), the quality of the human feature is improved. Siamese networks have two inputs and one output and are often used for person re-identification [30]–[32]. In this paper, the feature extractor is trained based on one of the Siamese networks [30]. The backbone network of the Siamese network is ResNet [33]. While the same human pair is annotated to “1”, a different human pair is annotated to “0”. While all training images are based on a normal rectangle without rectification in previous methods, in the proposed method, all training images are based on a rotated rectangle with local rectification.

3.2.3 Human Position Estimation in World Coordinates

The footpoint $\mathbf{q} = (q_1, q_2, 0)$ in the world coordinates is obtained from the query vector $\mathbf{n}$ through the estimator.

Table 2 LargeRoom dataset.

Sequence ID	1	2	3	4	5	6	7	8	9	10
Camera ID	1	2	1	2	1	2	1	2	1	2
The number of humans	6	6	6	6	6	6	6	6	6	6
Sequence length [sec]	180	180	180	180	180	180	180	180	180	180

Table 3 SmallRoom dataset.

Sequence ID	1	2	3	4	5	6	7	8
Camera ID	1	2	1	2	1	2	1	2
The number of humans	4	4	10	10	3	3	3	3
Sequence length [sec]	182	182	155	155	268	268	105	105

Algorithm 1 Algorithm of proposed method at frame f.

```
Input: : $\mathbf{o}^f$, $T^{f-1} = (\mathbf{t}_1^{f-1}, \mathbf{t}_2^{f-1}, \cdots, \mathbf{t}_{N_t}^{f-1})$
Output: : $T^f = (\mathbf{t}_1^f, \mathbf{t}_2,^f \cdots)$
  Calculate $B^f = (\mathbf{b}_1^f, \mathbf{b}_2^f, \cdots, \mathbf{b}_{N_b}^f)$
  for $j = 1$ to $N_b$ do
    Estimate $\mathbf{r}_j^f$ and $\mathbf{q}_j^f$ using the estimator.
    Extract $\mathbf{a}_j^f$ using the feature extractor.
  end for
  for $i = 1$ to $N_t$ do
    for $j = 1$ to $N_b$ do
      Calculate $c^{feat}(\mathbf{t}_i^{f-1}, \mathbf{b}_j^f)$ using $\mathbf{a}_j^f$.
      Calculate $c^{pos}(\mathbf{t}_i^{f-1}, \mathbf{b}_j^f)$ using $\mathbf{r}_j^f$.
    end for
  end for
  Apply the Hungarian algorithm to $C^{feat}$ and $C^{pos}$ for estimating $T_f$.
  Create new tracklets and delete tracklets.
```

3.3 Data Association

Multiple human tracking is performed by data association between the human tracking results at the previous frame and the bounding boxes at the current frame. $T^{f-1} = (\mathbf{t}_1^{f-1}, \mathbf{t}_2^{f-1}, \cdots, \mathbf{t}_{N_t}^{f-1})$ denotes tracklets at frame f, where $\mathbf{t} = (\mathbf{r}, id)$. In the algorithm, a cost matrix $C(T^{f-1}, B^f) \in \mathbb{R}^{N_t \times N_b}$ is calculated. $C(T^{f-1}, B^f)$ consists of $c(\mathbf{t}_i^{f-1}, \mathbf{b}_j^f)$ which is the cost between the tracklet $\mathbf{t}_i^{f-1}$ and the bounding box $\mathbf{b}_j^f$. Associated pairs are estimated by solving a linear assignment problem. It is solved efficiently using the Hungarian algorithm.

We calculate $c(\mathbf{t}_i^{f-1}, \mathbf{b}_j^f)$ based on feature/position, respectively. Therefore, we can obtain two cost matrices, C^{feat} based on feature and C^{pos} based on position. Although there are several ways of solving the linear assignment problem using two cost matrices, we introduce a two-step algorithm in this paper. First, we solve the linear assignment problem of C^{feat}. Second, for only unmatched tracking results in the first stage, the assignment is performed using C^{pos}. If $c(\mathbf{t}_i^{f-1}, \mathbf{b}_j^f)$ ¿ ε, $c(\mathbf{t}_i^{f-1}, \mathbf{b}_j^f) = \infty$ is set. ε is a predefined parameter, and it is separately prepared for feature ε_{feat} and position ε_{pos}.

3.4 Tracking Algorithm

The algorithm of the proposed method is shown in detail in Algorithm 1. The tracking algorithm was a simple online algorithm. The association algorithm and other handling (add/delete humans) were based on the DeepSORT algorithm [3].

4. Experiments

We conducted experiments on multiple human tracking in order to verify the effectiveness and efficiency of the proposed method.

4.1 Experimental Conditions

We made two datasets that were created under a variety of conditions in the rooms we used for our experiments. We used a Panasonic WV-SF438[†] fisheye camera as the omnidirectional camera. The image resolution of this camera is 1280 × 960 with a video frame rate of 15 [fps]. The camera parameters were calculated by calibration using OCamCalib[††]. For the LargeRoom dataset, the area of the room was about 128 [m^2] (8 [m] wide × 16 [m] long). For the SmallRoom dataset, the area of the room was about 36 [m^2] (4 [m] wide × 9 [m] long). The details of the datasets are shown in Tables 2 and 3.

For the human detector (SSD), we used the default hyper-parameters. The detector was trained using 220,874 images captured in various rooms including SmallRoom. For the data association parameter, we changed the two parameters, $\varepsilon_{feat} \in \{200, 300, 400\}$ and $\varepsilon_{pos} \in \{0.3, 0.5, 0.7, 0.9\}$. Then $\varepsilon_{feat} = 300$, $\varepsilon_{pos} = 0.7$ were determined using validation data.

The human detector was implemented in MXNet, and the feature extractor was implemented in PyTorch. We used a 4.20GHz Intel® Core™ i7-7700K CPU, a 32GB RAM, and a NVIDIA GeForce Titan X Pascal GPU.

For the evaluation metric, we used Multiple Object Tracking Accuracy (MOTA) metric. MOTA is a widely used and comprehensive metric that combines three error sources

[†] https://security.panasonic.com/products/wv-sf438/
[††] https://sites.google.com/site/scarabotix/ocamcalib-toolbox

Table 4 Summary of the tracking results (MOTA).

	Feature	Position	1 [fps]			15 [fps]		
			LargeRoom	SmallRoom	SmallRoom2	LargeRoom	SmallRoom	SmallRoom2
-	no rectification	-	8.4	51.0	54.5	−3.5	48.7	72.9
SORT [2]	-	rectangle in image	−10.5	24.5	47.0	−1.4	49.9	74.5
DeepSORT [3]	no rectification	rectangle in image	−4.3	30.9	49.2	6.0	**52.3**	**75.3**
Proposed	local rectification	-	10.2	51.8	54.3	−3.4	48.5	72.7
	-	position in world	8.1	53.1	54.8	−1.1	49.7	74.4
	local rectification	position in world	**11.7**	**53.3**	**55.7**	**6.6**	52.0	**75.3**

as follows:

$$MOTA = 1 - (FN + IDs + FP)/DET, \tag{3}$$

where FN, IDs, FP, and DET denote the total number false negatives, ID switches, false positives, and detections, respectively. The MOTA score ranges from $-\infty$ to 100. More details about these metrics are described in another paper [34]. For bounding boxes, since the ground truth used a normal rectangle, the proposed method estimated tracking results in the normal rectangle $\mathbf{n} = (x, y, w, h)$. We made the ground truths at 1 [fps] because the sequences include a large number of frames. Therefore, the tracking results were only evaluated for the annotated frames.

4.2 Evaluation of Multiple Human Tracking

We evaluated each proposed function and their combinations. Also, we verified that the proposed method solves the existing problems. A summary of the tracking results is shown in Table 4. The MOTA in the table is an average of all the sequences. For the feature, "without local rectification" or "with local rectification" was used. For the position, "rectangle in image coordinates" or "position in world coordinates" was used. More details are shown in Appendix A.

4.2.1 Local Rectification

We evaluated the effects of local rectification. Let us compare (no rectification & -) to (local rectification & -). First, we present the results for LargeRoom. At 1 [fps], MOTA improves +1.8 (8.4 vs 10.2). At 15 [fps], MOTA is almost the same (−3.5 vs −3.4). Next, we present the results for SmallRoom. At 1 [fps], MOTA improves +0.8 (51.0 vs 51.8). At 15 [fps], MOTA is almost the same (48.7 vs 48.5). Local rectification is was shown to be effective particularly at a low frame rate. Local rectification is just as effective as no rectification at a normal frame rate. At 1 [fps], local rectification is more effective in the case of LargeRoom than for SmallRoom. (LargeRoom:+1.8 vs SmallRoom:+0.8)

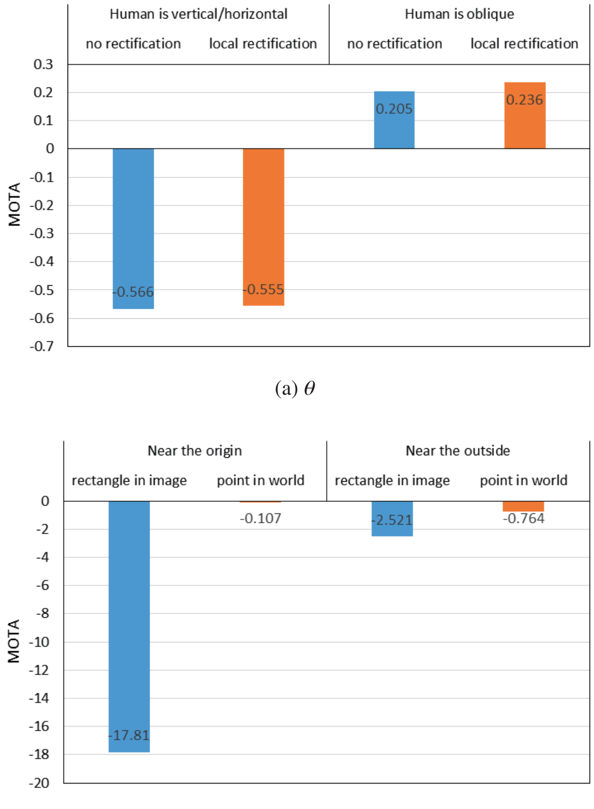

(a) θ

(b) r

Fig. 4 MOTA with respect to θ and r.

4.2.2 World Coordinates Representation

We then evaluated the world coordinates representation. Let us compare (- & rectangle in image) to (- & position in world). First, we present the results for LargeRoom. At 1 [fps], MOTA improves +18.6 (−10.5 vs 8.1). At 15 [fps], MOTA is almost the same (−1.4 vs −1.1). Next, we present the results for SmallRoom. At 1 [fps], MOTA improves +28.6 (24.5 vs 53.1). At 15 [fps], MOTA is almost the same (49.9 vs 49.7). The position in world coordinates is particularly effective at a low frame rate. The position in world coordinates is just as effective as the rectangle in image coordinates at a normal frame rate. At 1 [fps], the position in world coordinates is more accurate in the case of SmallRoom than for LargeRoom. (LargeRoom:+18.6 vs SmallRoom:+28.6)

4.2.3 Tendency Analysis

We analyzed those cases where the proposed method was particularly effective. The evaluation metric is MOTA which is regarded as the normalized ID switch. We used all sequences of all frame rates in the LargeRoom dataset. For analysis, the image coordinates (X, Y) are converted to the polar coordinates (θ, r). The center point $(640, 480)$ in the

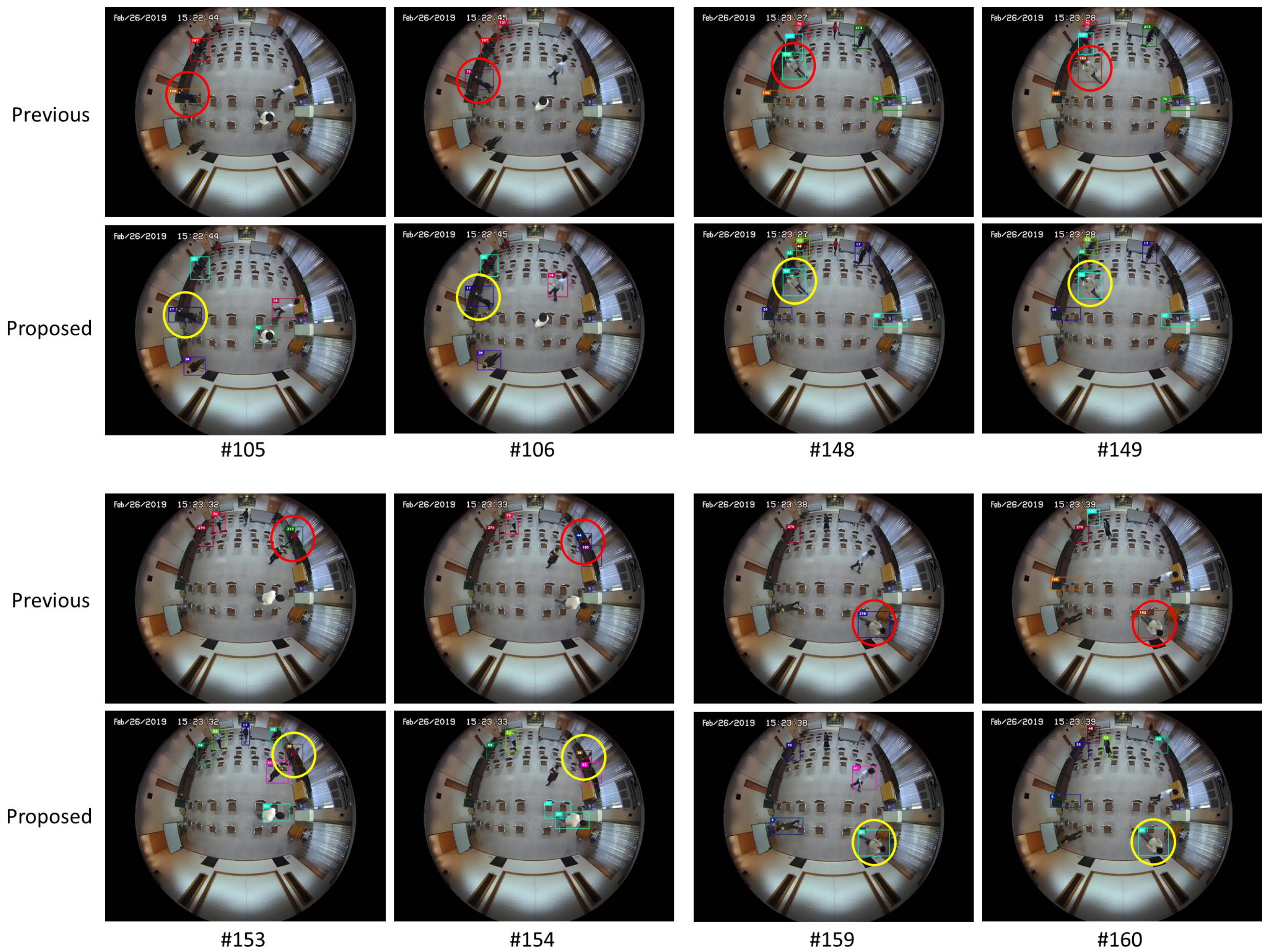

Fig. 5 Tracking examples. #(number) denotes the frame number. Red circles denote ID switch and yellow circles denote the prevention of ID switch.

image coordinates is set to point to the origin in the polar coordinates. θ [rad] is the angle made by the point of origin, and r [pixel] is the distance from the point of origin. Figure 4 shows the analysis results. The horizontal axis denotes θ and r, and the vertical axis denotes MOTA.

θ: We analyzed those cases where local rectification was particularly effective. Figure 4 (a) shows a comparison of MOTA between the cases where the human was vertical/horizontal ($-9/8\pi < \theta \leq -7/8\pi$, $-5/8\pi < \theta \leq -3/8\pi$, $-1/8\pi < \theta \leq 1/8\pi$, $3/8\pi < \theta \leq 5/8\pi$) and where the human was captured at an oblique angle ($-7/8\pi < \theta \leq -5/8\pi$, $-3/8\pi < \theta \leq -1/8\pi$, $1/8\pi < \theta \leq 3/8\pi$, $5/8\pi < \theta \leq 7/8\pi$)). When the human was vertical/horizontal, MOTA improved +0.011 (−0.566 vs −0.555). When the human was captured at an oblique angle, MOTA improved +0.031 (0.205 vs 0.236). Local rectification was more effective in the case where the human was captured at an oblique angle compared to the case where the human was vertical/horizontal. This is owing to background reduction.

r: We analyzed those cases where the world coordinates representation was particularly effective. Figure 4 (b) shows a comparison of MOTA between the case where the human was near the origin ($0 < r \leq 200$) and where the human was close to the outside ($300 < r \leq 500$). When the human was near the origin, MOTA improved +17.703 (−17.81 vs −0.107). When the human was close to the outside, MOTA improved +1.757 (−2.521 vs −0.764). The world coordinates representation was more effective in the case where the human was near the origin than where the human was close to the outside.

4.2.4 Local Rectification and World Coordinates Representation

We evaluated the combination of local rectification and world coordinates representation at 1 [fps] Let us compare (local rectification & -) to (- & position in world).

In the case of LargeRoom, local rectification was more effective than the world coordinates representation (10.2 vs 8.1). This is because local rectification is effective where the human is located around the outside of the image as described in Sect. 4.2.3. When combining local rectification with world coordinates representation, MOTA improved 1.5. This is because the world coordinates representation

Table 5 Computational time [msec].

Human detection	102.7
Rotated rectangle estimation	1.0
Human position estimation	0.7
Feature extraction	3.2
Data association	1.1

is effective where the human is located around the center of the image as described in Sect. 4.2.3.

In the case of SmallRoom, conversely, the world coordinates representation is more effective than local rectification (51.8 vs 53.3). This is because the world coordinates representation is effective in cases where humans are located around the center of the image as described in Sect. 4.2.3. However, combining local rectification and the world coordinates representation improved MOTA by only 0.2. The effectiveness of local rectification is low because the background area is small when humans are located around the center of the image.

Therefore, the proposed method (combining local rectification and the world coordinates representation) is effective, particularly in the case of a low frame rate (1 [fps]) and a large room (LargeRoom).

4.3 Evaluation of Computational Time

We evaluated the computational time needed for estimating rotated rectangles and human positions in the world coordinates. Table 5 shows the computational time which is the average of all frames in sequence 1 in the SmallRoom dataset. The computational times for rotated rectangles and human position estimation are 1.0 and 0.7 [msec], respectively. These times are very fast and have little impact on the overall tracking time. There are 4 humans in Sequence 1; therefore, it takes 0.25 [msec/human] to estimate the rotated rectangle and 0.18 [msec/human] to estimate the human position. The computational time needed for human detection accounts for a large percentage in the overall system. We can reduce it by employing other fast detectors or downsizing input images.

4.4 Tracking Examples

Some tracking examples are shown in Fig. 5. “Previous” denotes (no rectification & rectangle in image) and “Proposed” denotes (local rectification & position in world). #(number) denotes the frame number. Red circles denote ID switch and yellow circles denote the prevention of ID switch. ID switches are prevented in “Proposed” in some frames.

4.5 Discussion

We conducted an additional experiment using a more complex sequence in which more humans are moving freely. In the additional SmallRoom2 dataset, more humans (11) are moving in longer sequence lengths (169 [sec]), compared with sequences 3 and 4 in the SmallRoom dataset. The area of SmallRoom2 is the same as that of SmallRoom. The tracking results for SmallRoom2 are shown in Table 4. In addition to other datasets, the proposed method (combining local rectification and the world coordinates representation) is effective, particularly in case of a low frame rate (1 [fps]).

5. Conclusion

In this paper, we proposed a novel method that accurately tracks humans using an association metric for omnidirectional images. The key ideas of the proposed method are as follows: i) Reducing the background regions by local rectification. ii) Describing the human position in the world coordinate system. In the experiments, we confirmed that the proposed method is effective, particularly at a low frame rate. MOTA improved 3.3 in the LargeRoom dataset and MOTA improved 2.3 in the SmallRoom dataset. It takes only 0.43 [msec] per human in a frame to calculate the proposed association metrics. In the future, it will be important not only reducing background regions and normalize angles but also to capture human appearance itself. Additionally, the same idea as the proposed method will be generalized for standard cameras when perspective effects and lens distortions are quite noticeable.

References

[1] R.T. Collins, A.J. Lipton, T. Kanade, H. Fujiyoshi, D. Duggins, Y. Tsin, D. Tolliver, N. Enomoto, O. Hasegawa, P. Burt, et al., “A system for video surveillance and monitoring,” VSAM final report, pp.1–68, March 2000.

[2] A. Bewley, Z. Ge, L. Ott, F. Ramos, and B. Upcroft, “Simple online and realtime tracking,” Proceedings of the 23rd IEEE International Conference on Image Processing (ICIP), pp.3464–3468, Sept. 2016.

[3] N. Wojke, A. Bewley, and D. Paulus, “Simple online and realtime tracking with a deep association metric,” Proceedings of the 24th IEEE International Conference on Image Processing (ICIP), pp.3645–3649, Sept. 2017.

[4] C. Kim, F. Li, A. Ciptadi, and J.M. Rehg, “Multiple hypothesis tracking revisited,” Proceedings of the 15th IEEE International Conference on Computer Vision (ICCV), pp.4696–4704, Dec. 2015.

[5] Q. Chu, W. Ouyang, H. Li, X. Wang, B. Liu, and N. Yu, “Online multi-object tracking using cnn-based single object tracker with spatial-temporal attention mechanism,” Proceedings of the 16th IEEE International Conference on Computer Vision (ICCV), pp.4846–4855, Oct. 2017.

[6] A. Sadeghian, A. Alahi, and S. Savarese, “Tracking the untrackable: Learning to track multiple cues with long-term dependencies,” Proceedings of the 16th IEEE International Conference on Computer Vision (ICCV), pp.300–311, Oct. 2017.

[7] J. Son, M. Baek, M. Cho, and B. Han, “Multi-object tracking with quadruplet convolutional neural networks,” Proceedings of the 30th IEEE Conference on Computer Vision and Pattern Recognition (CVPR), pp.5620–5629, July 2017.

[8] L. Zhang, Y. Li, and R. Nevatia, “Global data association for multi--object tracking using network flows,” Proceedings of the 21st IEEE Conference on Computer Vision and Pattern Recognition (CVPR), pp.1–8, June 2008.

[9] S. Ren, K. He, R. Girshick, and J. Sun, “Faster R-CNN: Towards real-time object detection with region proposal networks,” IEEE Transactions on Pattern Analysis and Machine Intelligence, vol.39, no.6, pp.1137–1149, 2017.

[10] J. Redmon, S. Divvala, R. Girshick, and A. Farhadi, "You only look once: Unified, real-time object detection," Proceedings of the 29th IEEE Conference on Computer Vision and Pattern Recognition (CVPR), pp.779–788, June 2016.
[11] W. Liu, D. Anguelov, D. Erhan, C. Szegedy, S. Reed, C.Y. Fu, and A.C. Berg, "SSD: Single shot multibox detector," Proceedings of the 14th European Conference on Computer Vision (ECCV), vol.9905, pp.21–37, Oct. 2016.
[12] S. Gächter and T. Pajdla, "Motion detection as an application for the omnidirectional camera," Research Reports of CMP, Czech Technical University in Prague, Omnidirectional Visual System (7), pp.5–13, Jan. 2001.
[13] H. Liu, W. Pi, and H. Zha, "Motion detection for multiple moving targets by using an omnidirectional camera," Proceedings of the IEEE International Conference on Robotics, Intelligent Systems and Signal Processing (RISSP), pp.422–426, Oct. 2003.
[14] G. Cielniak, M. Miladinovic, D. Hammarin, L. Goranson, A. Lilienthal, and T. Duckett, "Appearance-based tracking of persons with an omnidirectional vision sensor," Proceedings of the 16th IEEE Conference on Computer Vision and Pattern Recognition (CVPR) Workshop, pp.84–84, June 2003.
[15] M. Kobilarov, G. Sukhatme, J. Hyams, and P. Batavia, "People tracking and following with mobile robot using an omnidirectional camera and a laser," Proceedings of the IEEE International Conference on Robotics and Automation (ICRA), pp.557–562, May 2006.
[16] C.J. Song, C.M. Huang, and L.C. Fu, "Human tracking by importance sampling particle filtering on omnidirectional camera platform," IFAC Proceedings Volumes, vol.41, no.2, pp.6496–6501, July 2008.
[17] A. Kawasaki, D.H. Hung, and H. Saito, "Human trajectory tracking using a single omnidirectional camera," Proceedings of the 16th Irish Machine Vision and Image Processing (IMVIP) Conference, pp.157–162, Aug. 2014.
[18] A. Delforouzi, S.A.H. Tabatabaei, K. Shirahama, and M. Grzegorzek, "Unknown object tracking in 360-degree camera images," Proceedings of the 23rd International Conference on Pattern Recognition (ICPR), pp.1798–1803, Dec. 2016.
[19] X. Chen and J. Yang, "Towards monitoring human activities using an omnidirectional camera," Proceedings of the 4th IEEE International Conference on Multimodal Interfaces (ICMI), pp.423–428, Oct. 2002.
[20] F. Rameau, D. Sidibé, C. Demonceaux, and D. Fofi, "Visual tracking with omnidirectional cameras: an efficient approach," Electronics letters, vol.47, no.21, pp.1183–1184, Oct. 2011.
[21] I. Cinaroglu and Y. Bastanlar, "A direct approach for object detection with catadioptric omnidirectional cameras," Signal, Image and Video Processing, vol.10, no.2, pp.413–420, Feb. 2016.
[22] Z. Zhang, P.L. Venetianer, and A.J. Lipton, "A robust human detection and tracking system using a human-model-based camera calibration," Proceedings of the 8th International Workshop on Visual Surveillance (VS), inria-00325644v1, Oct. 2008.
[23] J. Yao and J.M. Odobez, "Multi-camera multi-person 3D space tracking with MCMC in surveillance scenarios," Proceedings of the 10th European Conference on Computer Vision (ECCV) Workshop on Multi-camera and Multi-modal Sensor Fusion Algorithms and Applications (M2SFA2), inria-00326747v1, Oct. 2008.
[24] O. Ronneberger, P. Fischer, and T. Brox, "U-Net: Convolutional networks for biomedical image segmentation," Proceedings of the 18th International Conference on Medical Image Computing and Computer Assisted Intervention (MICCAI), pp.234–241, Oct. 2015.
[25] V. Badrinarayanan, A. Kendall, and R. Cipolla, "SegNet: A deep convolutional encoder-decoder architecture for image segmentation," IEEE Transactions on Pattern Analysis and Machine Intelligence (PAMI), vol.39, no.12, pp.2481–2495, Dec. 2017.
[26] Y. Nagai, D. Kamisaka, N. Makibuchi, J. Xu, and S. Sakazawa, "3D person tracking in world coordinates and attribute estimation with PDR," Proceedings of the 23rd ACM International Conference on Multimedia (ACMMM), pp.1139–1142, Oct. 2015.
[27] L. Chen, W. Wang, G. Panin, and A. Knoll, "Hierarchical grid-based multi-people tracking-by-detection with global optimization," IEEE Transactions on Image Processing (IP), vol.24, no.11, pp.4197–4212, June 2015.
[28] D. Scaramuzza, A. Martinelli, and R. Siegwart, "A toolbox for easily calibrating omnidirectional cameras," Proceedings of the IEEE/RSJ International Conference on Intelligent Robots and Systems (IROS), pp.5695–5701, Oct. 2006.
[29] J.L. Bentley, "Multidimensional binary search trees used for associative searching," Communications of the ACM, vol.18, no.9, pp.509–517, Sept. 1975.
[30] E. Ahmed, M. Jones, and T.K. Marks, "An improved deep learning architecture for person re-identification," Proceedings of the 28th IEEE Conference on Computer Vision and Pattern Recognition (CVPR), pp.3908–3916, June 2015.
[31] R.R. Varior, M. Haloi, and G. Wang, "Gated siamese convolutional neural network architecture for human re-identification," Proceedings of the 14th European Conference on Computer Vision (ECCV), vol.9912, pp.791–808, Oct. 2016.
[32] R.R. Varior, B. Shuai, J. Lu, D. Xu, and G. Wang, "A siamese long short-term memory architecture for human re-identification," Proceedings of the 14th European Conference on Computer Vision (ECCV), vol.9911, pp.135–153, Oct. 2016.
[33] K. He, X. Zhang, S. Ren, and J. Sun, "Deep residual learning for image recognition," Proceedings of the 29th IEEE Conference on Computer Vision and Pattern Recognition (CVPR), pp.770–778, June 2016.
[34] K. Bernardin and R. Stiefelhagen, "Evaluating multiple object tracking performance: The CLEAR MOT metrics," EURASIP Journal on Image and Video Processing, vol.2008, no.1, pp.1–12, Feb. 2008.

Appendix A: Details of Tracking Results

A summary of the tracking results is shown in Tables A· 1, A· 2, A· 3 and A· 4. We evaluated ID switches (IDs), FragMentation (FM), Recall (Rcll), Precision (Prcn), Multiple Object Tracking Accuracy (MOTA) and Multiple Object Tracking Precision (MOTP) The numbers of IDs and FM are the sum of the all sequences, respectively. Rcll, Prcn, MOTA, and MOTP are the average of all the sequences, respectively.

A.1 LargeRoom Dataset

No rectification vs Local rectification: Let us compare (no rectification & -) to (local rectification & -). In 1 [fps], MOTA improves (8.4 vs 10.2). This is because IDs decrease (1279 vs 1101) while retaining Recall and Precision. Local rectification is effective, particularly at a low frame rate. At 15 [fps], MOTA is almost the same (−3.5 vs −3.4).

Rectangle in image vs Position in world: Let us compare (- & rectangle in image) to (- & position in world). At 1 [fps], MOTA improves (−10.5 vs 8.1). This is because Recall and Precision are improved significantly (Recall: 13.9 vs 41.8, Precision: 42.2 vs 63.5). The position in world is effective, particularly at a low frame rate. At 15 [fps], MOTA is almost the same (−1.4 vs −1.1).

Previous method vs Proposed method: Let us compare (three previous method) to (local rectification & position in

Table A· 1 Details of tracking results on LargeRoom dataset with 1 [fps].

	Feature	Position	Rcll ↑	Prcn ↑	IDs ↓	FM ↓	MOTA ↑	MOTP ↑
-	no rectification	-	**48.9**	63.4	1279	1587	8.4	30.7
SORT [2]	-	rectangle in image	13.9	42.2	**592**	**638**	−10.5	**30.9**
DeepSORT [3]	no rectification	rectangle in image	23.1	52.2	669	911	−4.3	30.6
Proposed	local rectification	-	**48.9**	63.5	1101	1580	10.2	30.7
	-	position in world	41.8	63.5	1018	1384	8.1	30.6
	local rectification	position in world	44.3	**64.2**	814	1409	**11.7**	30.6

Table A· 2 Details of tracking results on SmallRoom dataset with 1 [fps].

	Feature	Position	Rcll ↑	Prcn ↑	IDs ↓	FM ↓	MOTA ↑	MOTP ↑
-	no rectification	-	73.2	80.0	247	432	51.0	**22.2**
SORT [2]	-	rectangle in image	46.3	76.2	397	547	24.5	**22.2**
DeepSORT [3]	no rectification	rectangle in image	52.5	77.4	352	520	30.9	22.1
Proposed	local rectification	-	**73.3**	80.1	211	434	51.8	**22.2**
	-	position in world	72.3	**81.2**	161	**424**	53.1	**22.2**
	local rectification	position in world	72.5	80.8	**117**	426	**53.3**	**22.2**

Table A· 3 Details of tracking results on LargeRoom dataset with 15 [fps].

	Feature	Position	Rcll ↑	Prcn ↑	IDs ↓	FM ↓	MOTA ↑	MOTP ↑
-	no rectification	-	**49.5**	63.4	2576	1606	−3.5	**30.7**
SORT [2]	-	rectangle in image	47.0	**64.7**	2422	1607	−1.4	30.6
DeepSORT [3]	no rectification	rectangle in image	48.4	64.3	1634	1593	6.0	30.6
Proposed	local rectification	-	**49.5**	63.4	2567	1604	−3.4	**30.7**
	-	position in world	47.6	64.5	2386	1601	−1.1	30.6
	local rectification	position in world	48.6	64.1	**1561**	**1584**	**6.6**	30.6

Table A· 4 Details of tracking results on SmallRoom dataset with 15 [fps].

	Feature	Position	Rcll ↑	Prcn ↑	IDs ↓	FM ↓	MOTA ↑	MOTP ↑
-	no rectification	-	**74.2**	79.7	427	**438**	48.7	**22.2**
SORT [2]	-	rectangle in image	73.4	**80.7**	347	450	49.9	22.1
DeepSORT [3]	no rectification	rectangle in image	74.0	80.2	**193**	441	**52.3**	**22.2**
Proposed	local rectification	-	**74.2**	79.7	435	**438**	48.5	**22.2**
	-	position in world	73.4	80.6	371	453	49.7	22.1
	local rectification	position in world	73.9	80.1	206	443	52.0	**22.2**

world). At 1 [fps], MOTA improves (8.4 vs 11.7). Combining local rectification and position in world is effective, particularly at a low frame rate. At 15 [fps], MOTA slightly improves (6.0 vs 6.6).

A.2 SmallRoom Dataset

No rectification vs Local rectification: Let us compare (no rectification & -) to (local rectification & -). At 1 [fps], MOTA improves (51.0 vs 51.8). This is because IDs decrease (247 vs 211) while retaining Recall and Precision. Local rectification is effective, particularly at a low frame rate. At 15 [fps], MOTA is almost the same (48.7 vs 48.5).

Rectangle in image vs Position in world: Let us compare (- & rectangle in image) to (- & position in world). At 1 [fps], MOTA improves (24.5 vs 53.1). This is because Recall and Precision are improved significantly (Recall: 46.3 vs 72.3, Precision: 76.2 vs 81.2). The position in world is effective, particularly at a low frame rate. At 15 [fps], MOTA is almost the same (49.9 vs 49.7).

Previous method vs Proposed method: Let us compare (three previous method) to (local rectification & position in world). At 1 [fps], MOTA improves (51.0 vs 53.3). Combining local rectification and position in world are effective, particularly at a low frame rate. At 15 [fps], MOTA is almost the same (52.3 vs 52.0).

Hitoshi Nishimura received the B.E. and M.E. degrees in engineering from Kobe University, Japan, in 2013 and 2015, respectively. He joined KDDI Research, Inc. in 2016 and has been engaged in the research of human tracking and action recognition. He entered Nagoya University in 2018. He is a member of ITE.

Naoya Makibuchi received the B.E. and M.E. degrees in engineering from Tokyo Institute of Technology, Japan, in 2009 and 2011, respectively. In 2011, he joined KDDI Co. Ltd. and has been engaged in the research and development of person tracking and augmented reality. He is a research engineer of the Software Integration Laboratory at KDDI Research, Inc.

Kazuyuki Tasaka received his B.E. degree from Niihama National College of Technology in 2002. and his M.E. and Ph.D. degree from Nara Institute of Science and Technology in 2004 and 2010, respectively. Since joining KDDI Research, Inc. in 2004, he has worked in the field of network architecture, communication protocols and context recognition. Now, he is a R&D manager in the Media Recognition Laboratory and is a member of IEICE and IPSJ.

Yasutomo Kawanishi received his BEng and MEng degrees in Engineering and a Ph.D. degree in Informatics from Kyoto University, Japan, in 2006, 2008, and 2012, respectively. He became a Post Doctoral Fellow at Kyoto University, Japan in 2012. He moved to Nagoya University, Japan as a Designated Assistant Professor in 2014. Since 2015, he has been an Assistant Professor at Nagoya University, Japan. His research interests are Computer Vision techniques, especially Pedestrian Detection, Tracking, and Retrieval, for surveillance and in-vehicle videos. He received the best paper award from SPC2009, and Young Researcher Award from IEEE ITS Society Nagoya Chapter. He is a member of IEICE, IIEEJ, and IEEE.

Hiroshi Murase received the B.Eng., M.Eng., and Ph.D. in engineering from Nagoya University, Japan. From 1980 to 2003 he was a research scientist at the Nippon Telegraph and Telephone Corporation (NTT). He has been a professor of Nagoya University since 2003. He was awarded the IEEE CVPR Best Paper Award in 1994, the IEICE Distinguished Achievement and Contributions Award in 2018. He received Shijyu-hosho (the Medal with Purple Ribbon) in 2012. His research interests include computer vision, pattern recognition, and multimedia information processing. He is a fellow of IEEE, and a fellow of IPSJ.